LA-UR-17-28980
Approved for public release; distribution is unlimited.

Title: Spherical Nanoindentation Stress-Strain Measurements of BOR-60 14YWT-NFA1 Irradiated Tubes

Author(s): Weaver, Jordan
Carvajal Nunez, Ursula
Krumwiede, David
Saleh, Tarik A.
Hosemann, Peter
Nelson, Andrew Thomas
Maloy, Stuart Andrew
Mara, Nathan Allan

Intended for: Report

Issued: 2017-11-29 (rev.1)

Spherical Nanoindentation Stress-Strain Measurements of BOR-60 14YWT-NFA1 Irradiated Tubes

Jordan S. Weaver[1]
Ursula Carvajal Nunez[2]
David Krumwiede[3]
Tarik A. Saleh[4]
Peter Hosemann[3]
Andy Nelson[2]
Stuart A. Maloy[5]
Nathan A. Mara[1]

[1]Center for Integrated Nanotechnologies, Los Alamos National Laboratory
[2]Materials Science and Technology-7, Los Alamos National Laboratory
[3]Nuclear Engineering, University of California, Berkeley
[4]Materials Science and Technology-16, Los Alamos National Laboratory
[5]Materials Science and Technology-8, Los Alamos National Laboratory

September 28, 2017

SUMMARY

Spherical nanoindentation stress-strain protocols were applied to characterize unirradiated and fast neutron irradiated nanostructured ferritic alloy (NFA) 14YWT and compared against Berkovich nanohardness and available tensile data. The predicted uniaxial yield strength from spherical, 100 and 5 micron radii, indentation yield strength measurements was 1100-1400 MPa which compares well with the predictions from Berkovich nanohardness, 1200 MPa, and available tensile data, ~1100 MPa. However, spherical indentation measurements predict an increase in the uniaxial yield strength of ~1 GPa while Berkovich nanohardness measurements predict an increase of only ~250 MPa. No tensile data exists on the irradiated condition. It is believed the difference in the predicted uniaxial yield strength between spherical and Berkovich nanoindentation are due to a low number of tests on the irradiated sample combined with the significant heterogeneity in the microstructure, the differences in sensitivity to sample preparation on the irradiated sample between the two indentation protocols , and/or in how strain localizes under the indenter with the possibility of dislocation channeling under Berkovich hardness indents leading to strain softening. Nanoindentation capabilities to test neutron irradiated samples in a radiological area were realized.

TABLE OF CONTENTS

SUMMARY 1

1. Introduction 4

2. Materials and Methods 5
   - 2.1 Samples 5
   - 2.2 Experiments 5
   - 2.3 Analysis 6

3. Results and Discussion 7
   - 3.1 Local microstructure and mechanical heterogeneities 7
   - 3.2 Comparison between different nanoindenters 8
   - 3.3 Radiation hardening measurements 9

4. Future Work 11

5. Acknowledgements 12

6. References 12

FIGURES

Figure 1. (a) Schematic illustrating the paradigm of throughput versus perceived quality for different mechanical testing techniques. The green arrow represents current efforts by the PI and colleagues to develop more quantitative spherical nanoindentation protocols for irradiated materials. (b) Example spherical indentation stress-strain curve with the indentation properties labeled: modulus, strength, and work-hardening ($Eind, Yind, Hind$), respectively 4

Figure 2. (a) Representative indentation stress-strain curves for 14YWT ODS steel with a 100 µm radius indenter. (1) is the nominal response while (2) is atypical. (b-c) The corresponding EBSD Inverse Pole Figure (IPF) maps with Image Quality (IQ) superimposed that shows the difference in the microstructure on the surface at the indentation site. A step size of 0.25-0.3 microns was used for EBSD. 7

Figure 3. (a) EBSD-IFP map after indentation, (b) EBSD-IQ map, (c) load-displacement, (d) indentation modulus-displacement, and (e) hardness-displacement plots. The average indentation modulus and hardness values are given for each column of indents: red – first column from the right in the matrix, gray – second column from the right close to the large grain region, and black – third column from the right in the coarse grain region. The average values for each test were taken from 450-500 nm depth. A step size of 0.25-0.3 microns was used for EBSD. 8

Figure 4. (a) Comparison of indentation stress-strain response with two different nanoindenter systems on the same sample. (b-c) EBSD IPF-IQ maps of the residual indents. A step size of 0.25-0.3 microns was used for EBSD. 9

Figure 5. Spherical nanoindentation stress-strain measurements of unirradiated and neutron irradiated samples with (a) 100 micron radius indenter and (b) 5 micron radius indenter. The solid gray line is the average indentation modulus between the two tests, and the dotted gray line is a 0.2% strain offset line used to determine the indentation yield strength. 10

Figure 6. Predicted uniaxial yield strength from spherical indentation yield strength and Berkovich nanohardness measurements on unirradiated and irradiated conditions. Unirradiated tensile values come from Ref. [26]. The Irradiated UCB value comes from Refs. [15, 16] and is taken at a depth of 500 nm. 11

TABLES

Table 1. Description of nanoindenter systems and test methods used. 5

Table 2: Estimated indentation moduli along different crystal directions of 14YWT. The indenter tip material, diamond, Young's modulus and Poisson's ratio are assumed to be 1140 GPa and 0.07, respectively. 6

Table 3. Average properties for spherical stress-strain measurements for both systems. The averages and standard deviations come from a total of 13 and 11 tests for the NanoXP and Tribo950, respectively. 9

Table 4. Radiation hardening measurements from spherical nanoindentation tests. The averages and standard deviations come from 6-11 tests. 10

Table 5. Radiation hardening measurements from Berkovich hardness measurements averaged over 200-250nm depth. The averages and standard deviations come from 8-12 tests. 10

1. Introduction

Nanoindentation offers a high throughput, low cost mechanical characterization method for irradiated materials. For example, significant throughput is gained by coupling ion-irradiation and nanoindentation to screen candidate materials. In the case of neutron irradiated materials which are still radioactive, the cost and dose can be significantly reduced by working with only small amounts of material. However, nanoindentation, namely hardness, is considered low quality data compared to traditional uniaxial (i.e., compression and tension) tests as shown schematically in Figure 1a. The current NEET project is focused on developing more quantitative nanoindentation protocols specifically for irradiated materials. This is accomplished through novel spherical indentation stress-strain protocols [1, 2]. These protocols provide an effective or indentation stress versus strain response that is related to a uniaxial stress-strain response. This includes quantification of an indentation modulus, yield strength, and work-hardening behavior illustrated in Figure 1b. To date, we have successfully applied these protocols to characterize the differences in mechanical response between microstructures containing He-bubbles and/or dislocation loops in ion irradiated tungsten [3, 4], length scale effects associated with twinning in high purity zirconium [5], and benchmarked these protocols against other small-scale mechanical test protocols on proton irradiated 304 stainless steel [6]. The current report presents indentation measurements on an advanced steel, nanostructured ferritic alloy (NFA) 14YWT, before and after fast neutron reactor irradiation at the BOR-60 reactor facility. These measurements differ from our previous work in two aspects: the volume probed contains multiple grains (polycrystalline) compared to single grain measurements and the radiation damage is in the form of neutrons instead of ions which presents additional procedural challenges for testing radiological samples.

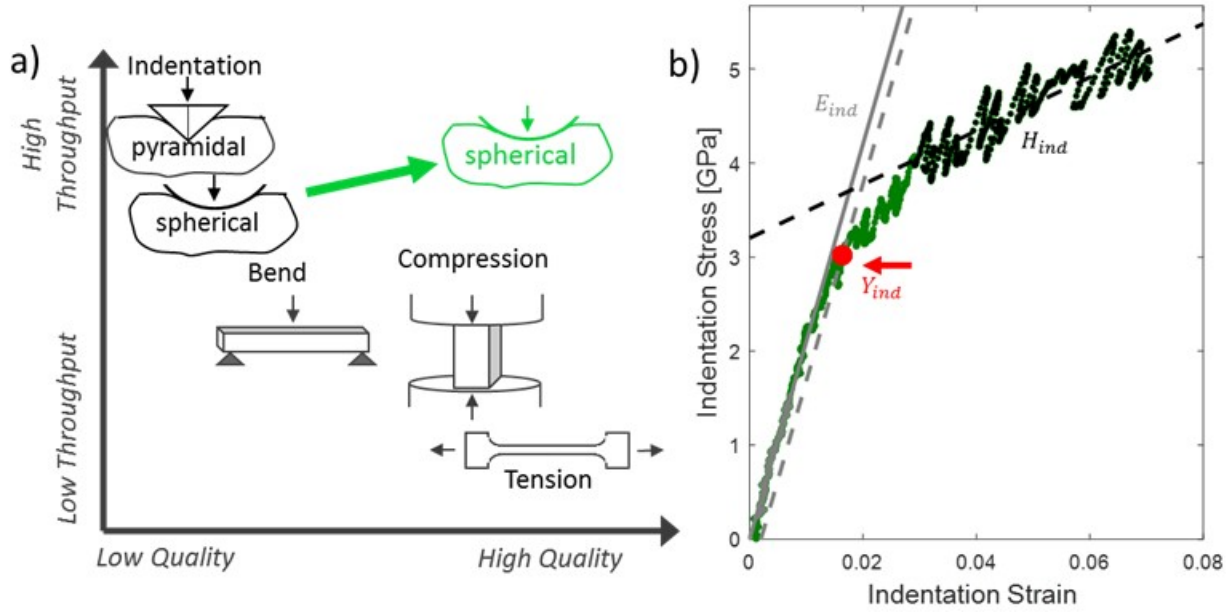

Figure 1. (a) Schematic illustrating the paradigm of throughput versus perceived quality for different mechanical testing techniques. The green arrow represents current efforts by the PI and colleagues to develop more quantitative spherical nanoindentation protocols for irradiated materials. (b) Example spherical indentation stress-strain curve with the indentation properties labeled: modulus, strength, and work-hardening ($E_{ind}, Y_{ind}, H_{ind}$), respectively.

2. Materials and Methods

2.1 Samples

The material tested was an oxide dispersion strengthened (ODS) nanostructured ferritic alloy (NFA) with a chemical composition of 12.8Cr- 2.95W-0.38Ti-0.22Y (wt.%) known as 14YWT [7]. This material system is one of the leading candidate materials for structural components in nuclear reactors due to its superior performance under the imposed extreme environment [8-12]. The material was manufactured through an extrusion and cross-rolling process designated as PM2 [13] and comes from a large ~10mm thick plate designed as NFA-1 [14]. Fast neutron irradiation was performed at the BOR-60 fast neutron reactor facility at a temperature of 360 °C to a displacement damage of 7 dpa [15, 16]. An unirradiated sample sectioned from the plate was metallographically prepared with a final vibratory polish using 0.05 micron colloidal silica. The irradiated sample was originally wire electrical discharged machined (EDM) from the NFA-1 plate into a tube prior to irradiation [16]. The tube axis lies along the plate rolling direction [16]. After irradiation, a small piece was sectioned from the tube and prepared with 0.1 μm diamond suspension so that nanoindentation could be performed along the tube axis direction. The unirradiated sample was mounted in epoxy while the irradiated sample was glued to a steel holder.

2.2 Experiments

Electron backscatter diffraction (EBSD) was performed on unirradiated samples using an FEI XL30 scanning electron microscope (SEM) and TSL EDAX Hikari detector to identify the microstructure at indentation sites. Nanoindentation was performed using several different indenters and tip geometries to determine the change in mechanical properties after irradiation. Two different nanoindenters were used to make the measurements on unirradiated samples, an MTS NanoXP Nano-indenter and a Hysitron Tribo950, and a third, separate nanoindenter located in a radiological area was used to test the neutron irradiated sample, a Hysitron Tribo900 upgraded with a Peformech digital controllwer so that the hardware was equivalent to the Tribo950 used for the unirradiated sample (see Table 1). All three indenters have a continuous stiffness measurement (CSM or CMX) module which allows for the continuous measurement of stiffness by applying a sinusoidal loading signal with a prescribed frequency and displacement or loading amplitude to generate many small elastic unloads. This is critical for determining the effective zero-point correction and evolution of contact area for the spherical nanoindentation protocols [2, 17]. The method or loading function used in all cases can be described as a constant strain rate method (loading rate divided by the load) to a prescribed depth. The CSM or CMX displacement amplitude was ~ 2nm in all cases and the frequency which depends in part on the indenter head/transducer was 45 Hz for the MTS NanoXP, 80 Hz for the Hysitron Tribo950 High Load Transducer, and 100 Hz for the Hysitron Tribo950 Low Load Transducer. Data was collected with three different tip geometries: Berkovich (pyramidal), spherical with a radius of 100 microns, and spherical with a radius of 5 microns.

Table 1. Description of nanoindenter systems and test methods used.

Manufacturer and Model	Head/Transducer	Diamond Indenter Tip(s)	Method Description
MTS NanoXP/ Keysight G200	XP	100 μm radius	Constant Strain Rate with CSM
		Berkovich	
Hysitron Tribo950 (non-radiological area)	High Load	100 μm radius 5 μm radius	Constant Strain Rate with CMX in open loop control
	Low Load	Berkovich	
Hysitron Tribo950 (radiological area)	High Load	100 μm radius 5 μm radius	Constant Strain Rate with CMX in open loop control
	Low Load	Berkovich	

2.3 Analysis

Berkovich nanoindentation tests were analyzed using the Oliver-Pharr method [18, 19] to determine the modulus and hardness. The modulus and hardness for each test was calculated as the average between 200 and 250 nm depth. The area function was calibrated from indents on fused silica. Spherical nanoindentation tests were analyzed following the indentation stress-strain protocols of Kalidindi and Pathak [2]. The indentation properties of indentation modulus, indentation yield strength, and indentation work-hardening are shown on Figure 1b. These are not to be confused with uniaxial stress-strain properties although there is a relationship between indentation and uniaxial stress-strain for these protocols [20, 21]. The relationship between indentation and uniaxial measurements is presented next.

Estimates for the indentation modulus, E_{ind}, can be calculated from available elastic constants [22] and theory for elastically anisotropic cubic materials from Vlassak and Nix [23, 24], Table 2. According to Vlassak and Nix [23, 24], the effective modulus, E_{eff}, is a combination of the indenter Young's modulus, E_i, and Poission's ratio, v_i and the polycrystalline average sample Young's modulus, $\widehat{E_s}$, Poisson's ratio, $\widehat{v_s}$, and anisotropy term, β, which depends on the crystal elastic constants and crystal orientation, according to Eqn. (1). Here, we denote the entire sample term as the indentation modulus, E_{ind}, according to Equation Eqn. (2). The estimated indentation moduli in Table 2 serve as a guide for the spherical nanoindentation stress-strain analysis.

$$\frac{1}{E_{eff}} = \frac{1}{\beta}\left(\frac{1-\widehat{v_s}^2}{\widehat{E_s}}\right) + \frac{1-v_i^2}{E_i} \quad (1)$$

$$E_{ind} = \beta \frac{\widehat{E_s}}{1-\widehat{v_s}^2} \quad (2)$$

Table 2: Estimated indentation moduli along different crystal directions of 14YWT. The indenter tip material, diamond, Young's modulus and Poisson's ratio are assumed to be 1140 GPa and 0.07, respectively.

Crystal Direction	β	$\frac{\widehat{E_s}}{1-\widehat{v_s}^2}$	E_{eff}	E_{ind}
(100)	0.959	245.5	195	235
(101)	1.008	245.5	204	248
(111)	1.024	245.5	206	251

Berkovich hardness measurements, H, were converted to uniaxial yield strength values, σ_{ys}, using Eqn. (3) which is an empirical relationship determined from a large set of Vickers hardness and tensile yield strength data on various unirradiated and irradiated steels [25]. Equation (3) assumes a relationship between Vickers hardness, HV, and Berkovich nanohardness as $HV = 94.5H$ due to the difference between the surface contact area used for a four sided pyramid for Vickers hardness and the projected contact area used for a three-sided pyramid for Berkovich hardness. Spherical indentation yield strength, Y_{ind}, was converted to uniaxial yield strength using Eqn. (4) which was derived from finite element simulations with an isotropic elastic-plastic model that follows J_2 flow theory [21].

$$\sigma_{ys} = 266.5H - 114 \quad (3)$$

$$\sigma_{ys} = \frac{Y_{ind}}{2} \quad (4)$$

3. Results and Discussion

3.1 Local microstructure and mechanical heterogeneities

A 100 micron radius indenter was chosen to provide a more homogenous response of the material that could be interpreted as a bulk, polycrystalline response. This is the case for most indents in regions with nanocrystalline (200-300 nm) grains as shown in Figure 2b. However, there are some large grain (several microns) regions in the microstructure as shown in Figure 2c. The indentation stress-strain response when the indenter falls in or near these large grain regions shows the same indentation yield strength as the nanocrystalline regions; however, the indentation work-hardening is significantly reduced, Figure 2a. Similarly, Berkovich nanohardness measurements inside and outside these large grain regions show a significant difference in the mechanical response as shown in Figure 3. In this case the hardness at a depth of 450-500 nm is ~ 5.10 GPa in the nanocrystalline region and ~2.69 GPa in the coarse grain region. It is not clear if this difference in mechanical response is because the large grains are structurally different (e.g., different oxide particle morphologies) compared to the nanocrystalline grains or simply because of the difference in the number of grain boundaries. This is a topic of on-going research.

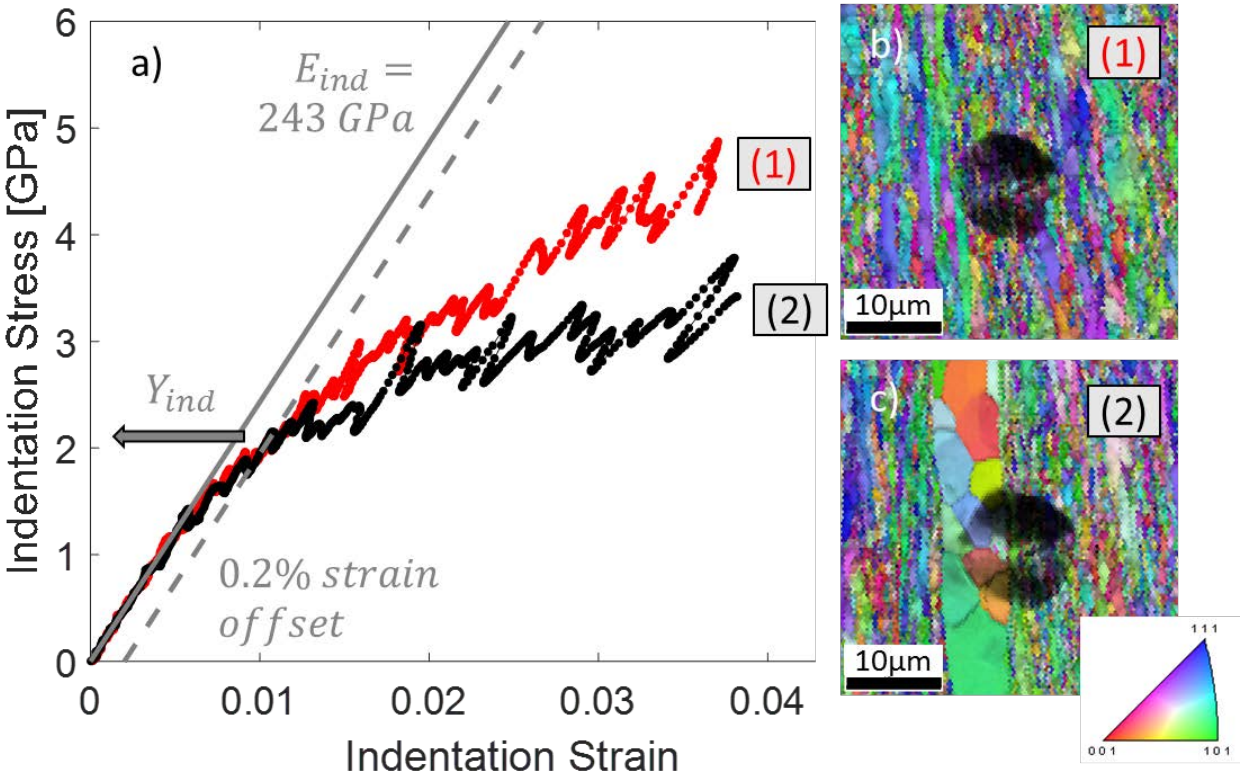

Figure 2. (a) Representative indentation stress-strain curves for 14YWT ODS steel with a 100 µm radius indenter. (1) is the nominal response while (2) is atypical. (b-c) The corresponding EBSD Inverse Pole Figure (IPF) maps with Image Quality (IQ) superimposed that shows the difference in the microstructure on the surface at the indentation site. A step size of 0.25-0.3 microns was used for EBSD.

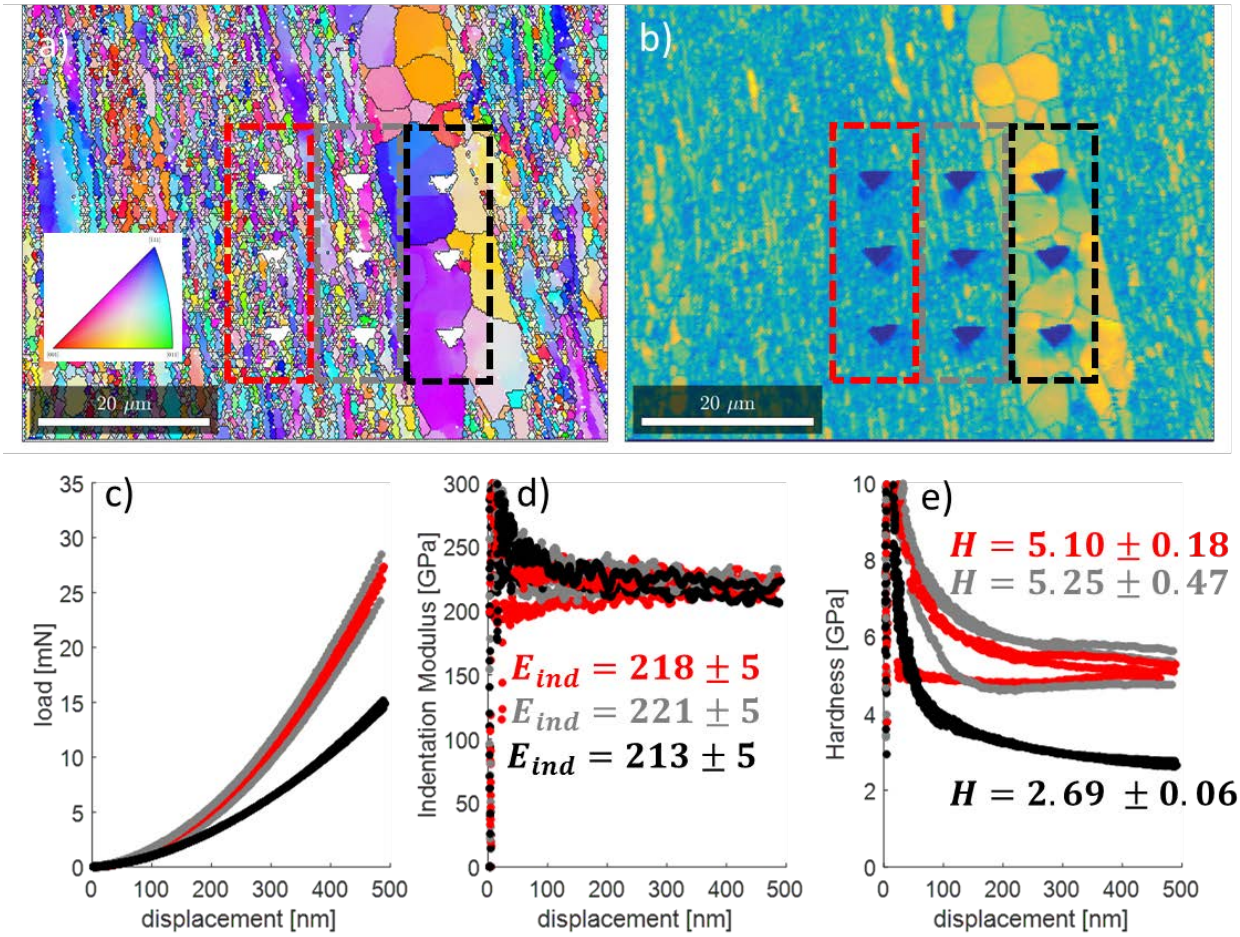

Figure 3. (a) EBSD-IFP map after indentation, (b) EBSD-IQ map, (c) load-displacement, (d) indentation modulus-displacement, and (e) hardness-displacement plots. The average indentation modulus and hardness values are given for each column of indents: red – first column from the right in the matrix, gray – second column from the right close to the large grain region, and black – third column from the right in the coarse grain region. The average values for each test were taken from 450-500 nm depth. A step size of 0.25-0.3 microns was used for EBSD.

3.2 Comparison between different nanoindenters

The current LANL indentation capability in a radiological area for testing neutron irradiated samples is limited to a Hysitron Tribo950. To date, the indentation stress-strain protocols [2] used in this work have only been employed using Keysight (Agilent and MTS) nanoindenters. The Hysitron nanoindenter is very different in the instrumentation and electronics; however, the general measurement procedure is the same. Figure 4 shows representative data from both nanoindenters on the same unirradiated sample with indenter tips with a nominal radius of 100 microns, and Table 3 lists the average properties. It is clear that both systems give the same result. The main differences between the two sets of data are the data collection frequency (higher for Tribo950) and the actual tip geometry. The nanoindenter tips are imaged by the manufacturers and specified to be nominally 100 microns in radius. This radius is used in the indentation stress-strain analysis. It is clear from Figure 4c that the Tribo950 tip has an asperity, particularly at larger depths, at which it becomes less spherical. It is our belief that this doesn't have a significant effect on the indentation yield strength measurement which occurs at very shallow depths.

Rather it produces some error in the indentation stress at larger strains (~0.03). In the future, this tip will be replaced with a more spherical probe.

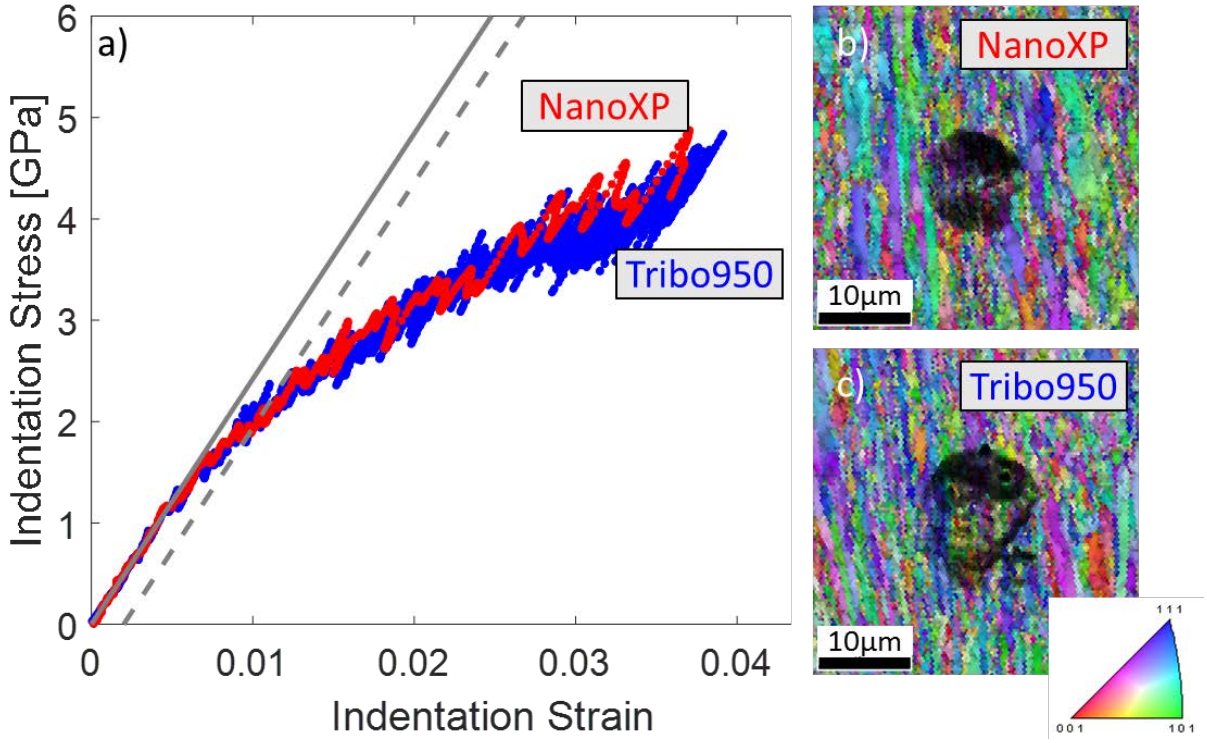

Figure 4. (a) Comparison of indentation stress-strain response with two different nanoindenter systems on the same sample. (b-c) EBSD IPF-IQ maps of the residual indents. A step size of 0.25-0.3 microns was used for EBSD.

Table 3. Average properties for spherical stress-strain measurements for both systems. The averages and standard deviations come from a total of 13 and 11 tests for the NanoXP and Tribo950, respectively.

System	Eind [GPa]	Yind [GPa]	Hind [GPa]
NanoXP	241 ± 6	2.20 ± 0.25	79.6 ± 17.6
Tribo950	245 ± 5	2.28 ± 0.11	72.8 ± 4.5

3.3 Radiation hardening measurements

Figure 5 shows representative spherical indentation stress-strain curves for 100 micron radius and 5 micron radius tips for the unirradiated and irradiated conditions. A second smaller indenter tip was chosen in order to collect indentation data at larger indentation strains (~10%). In this case the exact same tips were used for unirradiated and irradiated samples since it can be moved from the non-radiological indenter to the radiological indenter. Table 4 lists the average indentation modulus and indentation stress values for 100 μm radius and 5 μm radius spherical tips. The indentation stress from spherical tips is defined at three different strain offsets: 0.2% (indentation yield strength), 1%, and ~8-9% (at the end of the test). Table 5 list the Berkovich indentation modulus and hardness measurements averaged between 200 and 250 nm depth.

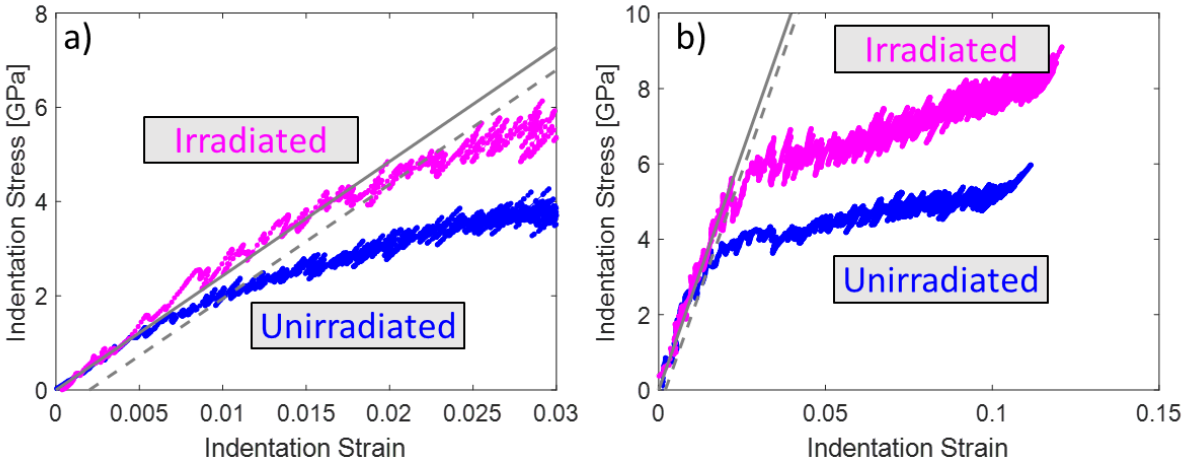

Figure 5. Spherical nanoindentation stress-strain measurements of unirradiated and neutron irradiated samples with (a) 100 micron radius indenter and (b) 5 micron radius indenter. The solid gray line is the average indentation modulus between the two tests, and the dotted gray line is a 0.2% strain offset line used to determine the indentation yield strength.

Table 4. Radiation hardening measurements from spherical nanoindentation tests. The averages and standard deviations come from 6-11 tests.

Condition	Indenter Type	Eind [GPa]	Indentation Yield (0.2% offset) [GPa]	Indentation Stress @ 1% offset [GPa]	Indentation Stress @ 8-9% offset [GPa]
Unirradiated	100 µm radius	245 ± 5	2.28 ± 0.11	3.46 ± 0.18	---
Irradiated	100 µm radius	242 ± 1	4.26 ± 0.33	5.80 ± 0.50	---
Unirradiated	5 µm radius	246 ± 5	2.77 ± 0.55	3.25 ± 0.69	5.18 ± 1.08
Irradiated	5 µm radius	250 ± 6	4.79 ± 0.69	5.58 ± 0.56	7.60 ± 0.52

Table 5. Radiation hardening measurements from Berkovich hardness measurements averaged over 200-250nm depth. The averages and standard deviations come from 8-12 tests.

Condition	Indenter	Eind [GPa]	Hardness [GPa]
Unirradiated	Berkovich	242 ± 7	5.03 ± 0.19
Irradiated	Berkovich	244 ± 6	6.0 ± 0.26

Two points need to be made before discussing the predicted tensile yield strengths from the data in Tables 4 and 5. The first is that the increase in the spherical indentation yield strength (radiation hardening) for the neutron irradiated sample is approximately 2 GPa for both tip sizes and remains around 2-2.5 GPa regardless of the strain offset (i.e., 0.2, 1, or 8-9%). Thus, we are fairly confident that the change in spherical indentation yield strength is not affected by the tip size or the definition of the indentation yield strength (i.e., 0.2% offset). The second point, is that the spherical indentation stress in the unirradiated material for the 5 micron radius tip at 8-9% strain, 5.18 ± 1.08 GPa (Table 4), is the same magnitude as the Berkovich hardness, 5.03 ± 0.19 (Table 5). This is indicative of the work-hardening of the material under the indenter tip that occurs for both tip geometries. This work-hardening behavior is clearly captured in the spherical indentation stress-strain curve, Figure 5b, between the indentation yield point and the indentation stress at 8-9% strain offset (end of the test); whereas, it is not directly observed from Berkovich nanoindentation tests. The point of comparing these two types of indentation tests on the unirradiated material is to show that the spherical indentation protocols capture and elastic loading modulus, elastic to plastic transition or indentation yield strength, and the early work-hardening behavior; and the magnitude of the spherical indentation stress will eventually approach the Berkovich hardness

value. In other words, they differ in the mechanical information given, but will converge on the mechanical behavior at 8-9% strain offset regardless of the indentation method used.

Figure 6 shows the predicted uniaxial yield strengths based on the data in Tables 4 and 5 using Eqns. (3) and (4) to convert indentation measurements to uniaxial yield strength. The unirradiated predictions for all three indentation measurements agree reasonably well with tensile measurements from literature [26]. However, there is a significant difference in the predicted yield strength from spherical and Berkovich tests on the irradiated material. Spherical indentation tests predict a ~ 1 GPa increase in uniaxial yield strength while Berkovich hardness measurements predict only a ~250 MPa increase in strength. It is not clear to us why this is the case, but we present three possible causes from the greatest contributing factor to the least. The first possibility is that our Berkovich hardness measurements fell in a soft region on the irradiated material. This seems likely given that previous reports of nanohardness on the same irradiated material are ~ 7 GPa at 500 nm depth [15, 16] also shown in Figure 6. This would give a predicted uniaxial yield strength of ~1750 MPa or an increase in uniaxial yield strength of 500 MPa, closer to the spherical indentation predictions. The second factor is that the spherical indentation protocols are highly sensitive to sample preparation [27] and the 0.1 μm diamond final polish on the irradiated sample may have left some deformation at the surface. This could increase the apparent indentation yield strength of the irradiated material. The third possibility is that strain softening could be occurring in Berkovich hardness tests on the irradiated sample due to dislocation channeling. This has been observed in transmission electron microscopy under Berkovich indents in ion irradiated ferritic Fe-Cr alloys [28]. The stress and strain fields under both indenters are highly heterogeneous; however, for the Berkovich indenter, the strain is arguably more concentrated compared to the spherical probes.

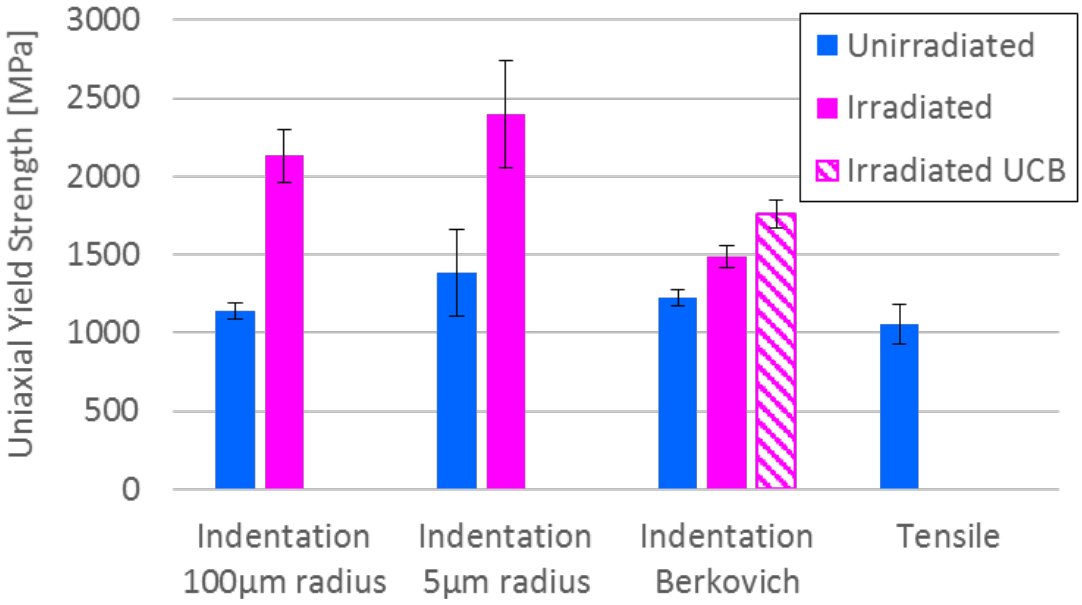

Figure 6. Predicted uniaxial yield strength from spherical indentation yield strength and Berkovich nanohardness measurements on unirradiated and irradiated conditions. Unirradiated tensile values come from Ref. [26]. The Irradiated UCB values come from Refs. [15, 16] and are taken at a depth of 500 nm.

4. Future Work

There are three outstanding questions from the work so far:

(1) How does the spherical nanoindentation mechanical response of ion irradiated material compare to fast neutron irradiated material? To answer this, we will be ion irradiating the same 14YWT

alloy under comparable conditions in temperature and dose to the neutron irradiated sample followed by indentation testing.

(2) Are the large grain regions mechanically and structurally different (e.g., different strength) than the nanocrystalline regions? This is being answered through small radius (1 micron) spherical indentation, Berkovich indentation, and TEM inside and outside the large grain regions.

(3) What is the cause for the difference in the radiation hardening measured from spherical indentation yield strength and Berkovich nanohardness measurements? EBSD on the irradiated sample would allow correlations between the grain structure and indents. In addition, TEM under spherical and Berkovich indents would hopefully provide evidence if dislocation channeling has occurred. Spherical indents to larger strains may also show strain softening if dislocation channeling occurs at higher strains.

5. Acknowledgements

The authors acknowledge funding from Department of Energy, Nuclear Engineering Enabling Technologies (DOE-NEET) - Reactor Materials program. This work was performed, in part, at the Center for Integrated Nanotechnologies, an Office of Science User Facility operated for the U.S. Department of Energy (DOE) Office of Science. Los Alamos National Laboratory, an affirmative action equal opportunity employer, is operated by Los Alamos National Security, LLC, for the National Nuclear Security Administration of the U.S. Department of Energy under contract DE-AC52-06NA25396.

6. References

[1] S. Pathak, S.R. Kalidindi. Spherical nanoindentation stress-strain curves, Mat Sci Eng R 91 (2015) 1-36.
[2] S.R. Kalidindi, S. Pathak. Determination of the effective zero-point and the extraction of spherical nanoindentation stress-strain curves, Acta Materialia 56 (2008) 3523-3532.
[3] J.S. Weaver, C. Sun, Y. Wang, S. Kalidindi, R. Doerner, N. Mara, S. Pathak. Quantifying the mechanical effects of He, W and He+W ion-irradiation on tungsten with spherical nanoindentation, J Mater Sci (submitted).
[4] S. Pathak, S.R. Kalidindi, J.S. Weaver, Y. Wang, R. Doerner, N.A. Mara. Probing nanoscale damage gradients in ion-irradiated metals using spherical nanoindentation, Scientific Reports (accepted).
[5] S. Pathak, S.R. Kalidindi, N.A. Mara. Investigations of orientation and length scale effects on micromechanical responses in polycrystalline zirconium using spherical nanoindentation, Scripta Materialia 113 (2016) 241-245.
[6] J.S. Weaver, S. Pathak, A. Reichardt, H.T. Vo, S.A. Maloy, P. Hosemann, N.A. Mara. Spherical nanoindentation of proton irradiated 304 stainless steel: A comparison of small scale mechanical test techniques for measuring irradiation hardening, J Nucl Mater 493 (2017) 368-379.
[7] E. Aydogan, S. Pal, O. Anderoglu, S.A. Maloy, S.C. Vogel, G.R. Odette, J.J. Lewandowski, D.T. Hoelzer, I.E. Anderson, J.R. Rieken. Effect of tube processing methods on the texture and grain boundary characteristics of 14YWT nanostructured ferritic alloys, Materials Science and Engineering: A 661 (2016) 222-232.
[8] R.L. Klueh, D.J. Alexander. Impact behavior of reduced-activation steels irradiated to 24 dpa, J Nucl Mater 233 (1996) 336-341.
[9] G.R. Odette, M.J. Alinger, B.D. Wirth. Recent Developments in Irradiation-Resistant Steels, Annual Review of Materials Research 38 (2008) 471-503.
[10] S. Ukai, S. Ohtsuka. Nano-mesoscopic structure control in 9Cr–ODS ferritic steels, Energy Materials 2 (2007) 26-35.

[11] G.R. Odette, D.T. Hoelzer. Irradiation-tolerant nanostructured ferritic alloys: Transforming helium from a liability to an asset, JOM 62 (2010) 84-92.
[12] G.R. Odette. Recent Progress in Developing and Qualifying Nanostructured Ferritic Alloys for Advanced Fission and Fusion Applications, JOM 66 (2014) 2427-2441.
[13] N. Cunningham, Y. Wu, G. Odette, D. Gragg, K. Fields, D. Hoelzer, S. Maloy. Characterization of the Final Precursor Alloy to a Larger Best Practice Heat of 14YWT, DOE Fusion Reactor Materials Program Semiannual Progress Report for the Period Ending December 31 (2012).
[14] N. Cunningham, Y. Wu, G. Odette, D. Hoelzer, S. Maloy. Characterization of a larger best practice heat of 14YWT in annealed powder, HIP consolidated and extruded forms, Fusion Materials Semiannual Progress Report for Period Ending June 30 (2013).
[15] T.A. Saleh, S.A. Maloy, E. Aydogan, M.E. Quintana, T.J. Romero. Characterization of BOR-60 Irradiated 14YWT-NFA1 Tubes. Los Alamos National Laboratory (LANL), 2017.
[16] T.A. Saleh, M.E. Quintana, T.J. Romero, C.A. Yablinsky, C.J. Rietema, J.A. Valdez, T.E. Steckley, D.L. Krumweide. Mechanical Testing of BOR-60 Irradiated FCRD-NFA1 Tubing. Los Alamos National Laboratory, 2017.
[17] S. Pathak, J. Shaffer, S.R. Kalidindi. Determination of an effective zero-point and extraction of indentation stress-strain curves without the continuous stiffness measurement signal, Scr Mater 60 (2009).
[18] W.C. Oliver, G.M. Pharr. Measurement of hardness and elastic modulus by instrumented indentation: Advances in understanding and refinements to methodology, J Mater Res 19 (2004) 3-20.
[19] W.C. Oliver, G.M. Pharr. An improved technique for determining hardness and elastic-modulus using load and displacement sensing indentation experiments, J Mater Res 7 (1992) 1564-1583.
[20] B.R. Donohue, A. Ambrus, S.R. Kalidindi. Critical evaluation of the indentation data analyses methods for the extraction of isotropic uniaxial mechanical properties using finite element models, Acta Materialia 60 (2012) 3943-3952.
[21] D.K. Patel, S.R. Kalidindi. Correlation of spherical nanoindentation stress-strain curves to simple compression stress-strain curves for elastic-plastic isotropic materials using finite element models, Acta Materialia 112 (2016) 295-302.
[22] G. Stoica, A. Stoica, M. Miller, D. Ma. Temperature-dependent elastic anisotropy and mesoscale deformation in a nanostructured ferritic alloy, Nature communications 5 (2014) 5178.
[23] J.J. Vlassak, W.D. Nix. Measuring the elastic properties of anisotropic materials by means of indentation experiments, Journal of the Mechanics and Physics of Solids 42 (1994) 1223-1245.
[24] J.J. Vlassak, W.D. Nix. Indentation Modulus of Elastically Anisotropic Half-Spaces, Philos Mag A 67 (1993) 1045-1056.
[25] T.S. Milot. Establishing Correlations for Predicting Tensile Properties Based on the Shear Punch Test and Vickers Microhardness data. University of California, Santa Barbara, 2012.
[26] M.E. Alam, S. Pal, K. Fields, S. Maloy, D.T. Hoelzer, G.R. Odette. Tensile deformation and fracture properties of a 14YWT nanostructured ferritic alloy, Materials Science and Engineering: A 675 (2016) 437-448.
[27] S. Pathak, D. Stojakovic, R. Doherty, S.R. Kalidindi. Importance of surface preparation on the nano-indentation stress-strain curves measured in metals, J Mater Res 24 (2009) 1142-1155.
[28] C.D. Hardie, S.G. Roberts. Nanoindentation of model Fe–Cr alloys with self-ion irradiation, J Nucl Mater 433 (2013) 174-179.